Magnetic Resonance Imaging 57 (2019) 1–7

Contents lists available at ScienceDirect

Magnetic Resonance Imaging

journal homepage: www.elsevier.com/locate/mri

Original contribution

Early assessment of acute kidney injury using targeted field of view diffusion-weighted imaging: An in vivo study

Hanjing Kong[a], Chengyan Wang[a], Fei Gao[b], Xiaodong Zhang[c], Min Yang[d], Li Yang[e], Xiaoying Wang[a,c,*], Jue Zhang[a,b,**]

[a] Academy for Advanced Interdisciplinary Studies, Peking University, 100871 Beijing, China
[b] College of Engineering, Peking University, 100871 Beijing, China
[c] Department of Radiology, Peking University First Hospital, 100034 Beijing, China
[d] Department of Interventional Radiology and Vascular Surgery, 100034 Beijing, China
[e] Renal Division, Peking University First Hospital, 100034 Beijing, China

ARTICLE INFO

Keywords:
Diffusion-weighted imaging
Targeted field-of-view
Acute kidney injury

ABSTRACT

Acute kidney injury (AKI) is a common complication in various clinical settings. In recent years, AKI diagnostics have been investigated intensively showing the emerging need for early characterization of this disease. To verify whether targeted field-of-view diffusion-weighted imaging (tFOV-DWI) is feasible to significantly improve the performance of traditional full field-of-view diffusion-weighted imaging (fFOV-DWI) in the early assessment of AKI. 14 rabbits with unilateral AKI were induced by injection of microspheres under the guidance of digital subtraction angiography (DSA). All rabbits underwent tFOV-DWI and fFOV-DWI immediately after the surgery. Artifacts, distortion and lesion identification were graded by two experienced radiologists, and the signal-to-noise ratio (SNR) and contrast-to-noise ratio (CNR) were measured. Apparent diffusion coefficient (ADC) maps were then derived. Blood samples were collected pre- and post-surgery and serum creatinine weres measured. Renal specimen and biopsy were performed as the reference standard. Student *t*-test was used to ascertain statistical significance between the above parameters for tFOV-DWI and fFOV-DWI. The interobserver agreement and ADC measurements agreement were assessed. A higher percentage of renal lesions (17 out of 19) were detected in tFOV-DWI compared with fFOV-DWI (14 out of 19). Significant differences were observed in ADC value for both techniques between the lesion regions and normal tissues ($p < 0.001$). Histological findings were inversely correlated with ADC values of tFOV-DWI ($r = -0.97$, $P < 0.001$ for cortex; $r = -0.98$, $P < 0.001$ for medulla) and fFOV-DWI sequences ($r = -0.95$, $P < 0.001$ for cortex; r = −0.98, $P < 0.001$ for medulla). Those tFOV-DW images rated by the radiologists exhibit superior performance in terms of all assessed measures ($P < 0.05$), and interobserver agreement was excellent (ICC, 0.78 to 0.92). Besides, the ADC values derived from tFOV-DWI had a satisfactory agreement with those estimated by fFOV-DWI. The animal study demonstrates that the tFOV-DWI strategy provided visually better image quality and lesion depiction than conventional fFOV-DWI for early assessment of AKI.

1. Introduction

Acute kidney injury (AKI) is a common complication in various clinical settings [1], characterized by a sudden loss of renal excretory function. Generally, AKI is associated with poor prognosis and adverse outcomes and may lead to chronic kidney disease [2–4]. In recent years, AKI diagnostics have been investigated intensively showing the emerging need for early characterization of this disease. The concentration of serum creatinine is the most widely used and commonly accepted measure of acute kidney injury in clinical medicine. However, serum creatinine is highly influenced by age, gentle and preexisting renal impairment, and only significantly altered if potentially irreversible kidney damage is present [5].

Noninvasive monitoring of AKI in an early stage is difficult because available techniques for detecting AKI are limited. Previous studies have shown that changes in renal diffusion, hemodynamics and perfusion are key factors in the progression of AKI [6–8]. With the development of magnetic resonance (MR) imaging, Diffusion-weighted

* Correspondence to: X. Wang, 8 Xishiku Street, Peking University First Hospital, Department of Radiology, Beijing 100034, China.
** Correspondence to: J. Zhang, 5 Yiheyuan Rd, Peking University, College of Engineering, Beijing 100871, China.
E-mail addresses: cjr.wangxiaoying@vip.163.com (X. Wang), zhangjue@pku.edu.cn (J. Zhang).

https://doi.org/10.1016/j.mri.2018.10.012
Received 7 June 2018; Received in revised form 9 October 2018; Accepted 18 October 2018

imaging (DWI) has rapidly grown and plays an important role in the assessment of renal dysfunction non-invasively and quantitatively. DWI characterizes the random Brownian motion of water molecules and numerous studies have characterized renal dysfunction including acute kidney injury using DWI [9–12].

The single shot EPI is the most commonly used sequence in abdominal DWI imaging. However, traditional single shot DWI suffers from problems of severe geometric distortion and artifacts [13] due to the susceptibility originated from gradients and long echo train length (ETL), and the spatial resolution is quite limited due to the single-shot EPI acquisition scheme. The low bandwidth of each pixel in the phase encoding direction and long EPI readout also result in blurring with single-shot EPI [14]. These may easily lead to inaccuracy in lesion evaluation, especially for small-sized lesions [15]. DWI techniques that are less sensitive to susceptibility artifacts and have high image resolution are highly desired in the clinic. In many previous studies, to improve the DWI image quality and reduce artifacts, several strategies including parallel imaging [16–18], reduced field-of-view (FOV) imaging [19–23] and multi-shot DWI have been proposed and gained promising results.

Recently, DWI has seemed to have a huge chance to benefit from reduced FOV imaging techniques. One of the reduced FOV DWI approaches targeted FOV-DWI, used 2D radiofrequency (RF) pulse for spatially selective excitation, in which the decreased number of k-space lines could shorten the ETL of EPI and decrease susceptibility and chemical shift artifacts [24]. The reduced acquisition time can be further exploited to achieve higher spatial resolution and alleviate partial volume effect, which may be potentially beneficial for small lesion detection [25] in an early stage.

14 rabbits were included in this study. Unliteral acute kidney injury models were induced under the guidance of digital subtraction angiography (DSA) and confirmed by serum creatinine reduction and histological findings. 2D excitation RF pulse combined tFOV-DWI was adopted for renal evaluation right after renal surgery and further compared with fFOV-DWI in the aspects of artifacts, distortion, ADC values as well as lesion depiction. The student *t*-test, ICC and Bland-Altman analysis were used for quantitative comparison.

The aim of this study is to compare image quality and lesion depiction of tFOV-DWI with fFOV-DWI and to evaluate the performance of tFOV-DWI for early assessment of AKI in animal models.

2. Material and methods

2.1. Subjects

The study was approved by the local Institutional Review Board. Fourteen New Zealand white rabbits (male, 3.09 ± 0.58 kg) underwent unilateral acute kidney injury induced by injection of microsphere through renal artery under the guidance of DSA. All the rabbits were given standard rabbit diet and tap water, and the animals were housed individually under the same conditions.

2.2. Unilateral acute kidney injury

In the experiment of renal embolization, rabbits were anesthetized by injection with a dose of 0.5 mg/kg pentobarbital sodium through the ear vein before surgery. Unilateral acute kidney injury was induced by injection of microsphere through the right renal artery (50,000 doses, acryl beads, 40–120 μm in diameter), and the DSA was then implemented to confirm the success of the unilateral artery embolization. The rabbits' body temperature was maintained about 38° before MR scan, and blood was collected by standard venipuncture into an evacuated blood collection tube without additives before and after surgery, and the serum creatinine was measured.

Table 1
Imaging parameters for fFOV-DWI and tFOV-DWI.

Sequence parameter	fFOV-DWI	tFOV-DWI
TR/TE (m*sec*)	3000/55	3000/55
FOV (mm)	150 × 150	80 × 150
Matrix	98 × 80	88 × 80
Number of averages	2	2
Thickness/gap (mm)	5/1	5/1
Bandwidth (kHz)	250	250
Resolution (mm)	1.5 × 1.9	0.9 × 1.9
b-Value (sec/mm^2)	0,1000	0,1000
Sense factor	2.0	2.0
Scan time(s)	120	120

TR = repetition time, TE = echo time, FOV = field of view.

2.3. MRI protocol

MRI was performed on a 3T clinical MRI system (Achieva, Philips Medical Systems, Best, The Netherlands) with a maximum gradient strength of 80 mT/m and a slew rate of 200 T/m/s. An 8-channel knee coil was used. After the unilateral renal artery embolization operation, the rabbits were immediately moved to the MR table to collect MRI data. Rabbits were anesthetized by injection with a dose of 0.5 mg/kg of pentobarbital sodium through the ear vein before scanning. T2 weighted images, fFOV-DWI, and tFOV-DWI were scanned. For DWI acquisition, two b values (0 and 1000 s/mm^2) were applied along all gradient directions to obtain the images. Other imaging parameters are listed in Table 1. All rabbits were scanned by the same technologist on the same scanner.

2.4. Histology

Under sterile conditions, kidneys were taken off for pathological examinations. Kidneys tissues were fixed in 10% formalin and embedded in paraffin for light microscopic observation. Kidneys were sectioned into 2-mm slides and stained with hematoxylin-eosin-saffron. A pathologist specializing in kidney diseases reviewed histological findings. The pathologist was blinded to the imaging findings and the results of pathology and renal specimen were considered as a reference standard for assessing the kidney injury.

2.5. Image analysis

2.5.1. Subjective assessment of image quality

Evaluation of the anonymized images was carried out. All data were interpreted by two radiologists in a blind, randomized fashion (reader A: 10 years of experience in abdominal MRI, reader B: 12 years of experience in abdominal MRI). Both readers scored those fFOV-DWI and tFOV-DWI images independently in terms of degree of susceptibility artifacts, distortion, and lesion identification according to a score rating systems (0–3): 0 = non-diagnostic; 1 = present, impeded image interpretation; 2 = present, irrelevant for image interpretation; 3 = excellent image quality.

2.5.2. Objective assessment of image quality

The signal to noise ratio (SNR) and contrast to noise ratio (CNR) in cortex and medulla were calculated and compared between fFOV-DWI and tFOV-DWI.

The SNR was defined as follows:

$$SNR_{cortex} = \frac{S_{lesion-cortex}}{SD_{background}},$$

$$SNR_{medulla} = \frac{S_{lesion-medulla}}{SD_{background}},$$

where SNR_{cortex} is signal to noise ratio in the cortex, $SNR_{medulla}$ is signal

to noise ratio in the medulla, $S_{lesion-cortex}$ is the mean signal intensity inside the cortex lesion, $S_{lesion-medulla}$ is the mean signal intensity inside the medulla lesion, $SD_{background}$ is the standard deviation of background noise.

The CNR was defined as follows:

$$CNR_{cortex} = \frac{|S_{lesion-cortex} - S_{normal-cortex}|}{\sqrt{SD_{lesion-cortex}^2 + SD_{normal-cortex}^2}},$$

$$CNR_{medulla} = \frac{|S_{lesion-medulla} - S_{normal-medulla}|}{\sqrt{SD_{lesion-medulla}^2 + SD_{normal-medulla}^2}},$$

where CNR_{cortex} is contrast to noise ratio in cortex, $CNR_{medulla}$ is contrast to noise ratio in medulla, $S_{lesion-cortex}$ is the mean signal intensity of the cortex lesion, $S_{lesion-medulla}$ is the mean signal intensity of the medulla lesion, $S_{normal-cortex}$ is the mean signal intensity of normal cortex, $S_{normal-medulla}$ is the mean signal intensity of normal medulla, $SD_{lesion-cortex}$ is the standard deviation of the cortex lesion, $SD_{lesion-medulla}$ is the standard deviation of the medulla lesion, $SD_{normal-cortex}$ is the standard deviation of normal cortex, $SD_{normal-medulla}$ is the standard deviation of the normal medulla.

2.5.3. Quantitative ADC assessment of acute kidney injury

For all experiments, mono-exponential ADC parameter maps were calculated and assessed based on signal intensity as a mono-exponential function of b-value according to ADC = $-\log(S_{1000}/S_0)/1000$, where S_0 is the signal intensity for b = 0 and S_{1000} is the signal intensity for b = 1000. Lesion and normal tissue contours were delineated on DWI images by reader A and saved as binary masks. Pixels inside contours were set to 1, the others to 0. T2W images were used as a guide to lesion and tissue locations. The delineated masks were loaded and multiplied with corresponding ADC map. The mean and standard deviation of ADC values in different region of interest of the lesion and tissue were calculated. All the calculations were performed using Matlab (MathWorks, Natick, MA).

2.6. Statistical analysis

Data were analyzed using SPSS 19.0.0 (SPSS Inc., Chicago, IL, USA) software and expressed as the mean ± standard deviation (SD). Differences between image scores, SNR, CNR and ADC values between tFOV-DWI and fFOV-DWI were tested using the paired *t*-test. Interobserver agreements for all subjective image quality features were assessed using the intraclass correlation coefficient (ICC) test. An ICC of 0.00 to 0.39 indicated poor, 0.40 to 0.59 fair, 0.60 to 0.74 good, 0.75 to 1.00 excellent agreement [26]. ADC values derived from fFOV-DWI and tFOV-DWI were analyzed by *t*-test and Bland-Altman analysis. ADC values between lesions and normal tissues were compared by *t*-test and the correlation between ADC values and histological findings was analyzed by Spearman rank correlation. $P < 0.05$ was considered significant.

3. Results

Subjective and objective image quality evaluations were listed in Tables 2 and 3, respectively. There were significant differences in the artifacts, distortion and lesion depiction between fFOV-DWI and tFOV-DWI for both readers ($P < 0.001$–0.030). Typical images for subjective image quality assessment are shown in Fig. 1.

The mean SNR_{cortex} and $SNR_{medulla}$ values of tFOV-DWI were significantly higher than that of fFOV-DWI (100.21 ± 38.60 vs 69.21 ± 24.62, $P = 0.005$ for cortex, 55.50 ± 23.11 vs 36.71 ± 15.68, $P = 0.047$ for medulla). The mean CNR_{cortex} and $CNR_{medulla}$ values of tFOV-DWI were comparable to that of fFOV-DWI (fFOV-DWI vs tFOV-DWI: 2.98 ± 1.85 vs 2.57 ± 1.86, $P = 0.538$ for cortex; 2.93 ± 1.81 vs 4.16 ± 1.80, $P = 0.103$ for medulla).

A total of 19 lesions were found 12 of the 14 rabbits by the renal specimen and confirmed by histological findings. 14 and 17 lesions were found by fFOV-DWI and tFOV-DWI, respectively. All lesion sizes were listed in Table 4. The area of 3 lesions that missed out by fFOV-DWI but identified by tFOV-DWI was 0.13, 0.05 and 0.09 cm^2. Typical lesion depiction comparisons are shown in Fig. 2. For the first severe injury case (Fig. 2 a), clear lesion margin and strong contrast between lesion and normal tissue were observed in tFOV-DWI. Compared to fFOV-DWI, higher resolution and reduced partial volume effect enabled precise visualization of lesions and helped avoid underestimation of lesion size in tFOV-DWI images. In another severe injury case (Fig. 2 b), renal injury with low signal intensity was easily identified in tFOV-DW image. While in fFOV-DWI image, no obvious signal intensity changes in the lesion region. Besides, abnormal high-intensity signals caused by susceptibility change near renal pelvis edge and renal bottom edge were reduced in tFOV-DWI images. For the third case (Fig. 2. c), lesions were distributed at the bottom left of renal. Since the image exhibited poor quality with low image resolution and blurred renal edge, it is difficult to determine renal injury by fFOV-DWI. However, on tFOV-DWI images, multiple, abnormal, high-intensity signal lesions were found in the area along the left edge of renal and were confirmed by histological results.

The quantitative ADC values of normal tissues and lesions were analyzed and the results were listed in Tables 5 and 6. Significant differences were found between the ADC values of lesions and normal tissues for fFOV-DWI and tFOV-DWI in cortex and medulla ($P < 0.001$). No significant differences were found between fFOV-DWI and tFOV-DWI in medulla lesion, cortex lesion, normal medulla lesion and normal cortex tissue ($P = 0.07$–0.14). Bland-Altman analysis results of accordance between ADC values were illustrated in Fig. 3. An inverse correlation was noted between ADC values and histological findings for both tFOV-DWI and fFOV-DWI (Table 7).

Interobserver agreement for the fFOV-DWI and tFOV-DWI sequences was excellent for artifacts, distortion and lesion depiction. The

Table 2
Subjective image quality assessment.

Image score	Reader	fFOV-DWI	tFOV-DWI	*P* value[a]
Artifacts	Reader 1	2.15 ± 0.31	2.42 ± 0.31	0.003*
	Reader 2	2.17 ± 0.24	2.51 ± 0.30	< 0.001*
Distortion	Reader 1	2.29 ± 0.35	2.44 ± 0.30	0.003*
	Reader 2	2.24 ± 0.33	2.39 ± 0.27	0.010*
Lesion depiction	Reader 1	2.27 ± 0.22	2.46 ± 0.33	0.007*
	Reader 2	2.31 ± 0.24	2.48 ± 0.35	0.030*
Diagnostic		14	17	
Non-diagnostic		5	2	

$n = 14$ for all comparison.
fFOV-DWI and tFOV-DWI indicates full FOV DWI and targeted FOV DWI, respectively.
[a] Paired *t*-test to compare fFOV-DWI with tFOV-DWI (*indicates significant *P*-values).

Table 3
SNR and CNR comparisons between fFOV-DWI and tFOV-DWI.

	Cortex ($n = 10$)		Medulla ($n = 7$)	
	SNR	CNR	SNR	CNR
fFOV-DWI	100.21 ± 38.60	2.98 ± 1.85	55.50 ± 23.11	2.93 ± 1.81
tFOV-DWI	69.21 ± 24.62	2.57 ± 1.86	36.71 ± 15.68	4.16 ± 1.80
P value[a]	0.005*	0.538	0.047*	0.103

fFOV-DWI and tFOV-DWI indicate full FOV DWI and targeted FOV DWI, respectively.
SNR and CNR indicate signal-to-noise ratio and contrast-to-noise ratio, respectively.
[a] Paired *t*-test to compare fFOV-DWI with tFOV-DWI (*indicates significant *P*-values).

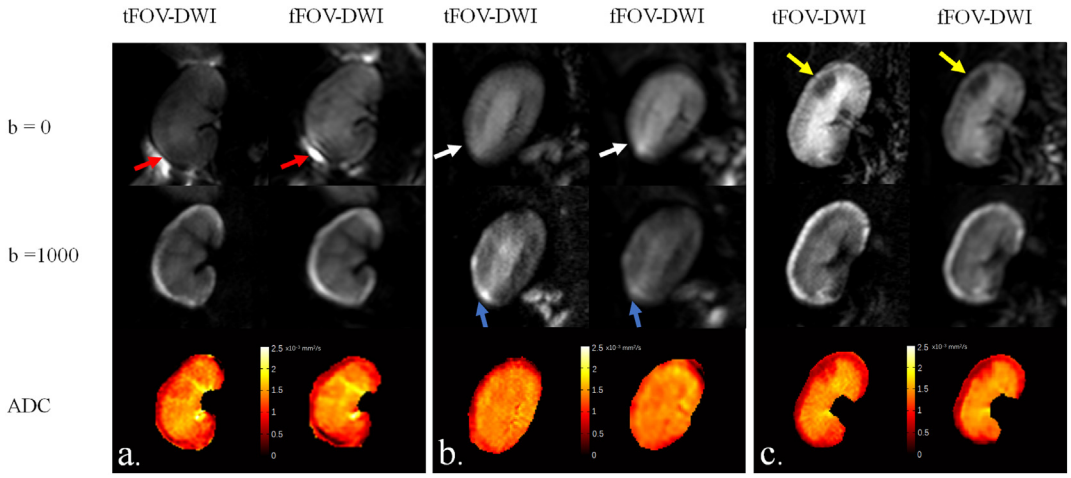

Fig. 1. Typical images for subjective image quality assessment. Typical comparisons of image artifact (a), distortion (b), and lesion identification (c). a: fFOV-DWI shows severe susceptibility artifacts (red arrow) produced at the same location with noticeable distortions. The image quality score for artifacts is 1.5. tFOV-DWI shows mild susceptibility artifacts (red arrow) adjacent to the bottom left edge of the renal without obvious distortions. The image quality score for artifacts is 2.8. b: fFOV-DWI shows the blurred wall of the lower margin of the renal with moderate distortion (white arrow). The image quality score for distortion is 2.0. tFOV-DWI shows the smooth and clear wall of the renal with mild distortion (white arrow). The image quality score for distortion is 2.5. The lesions are better depicted in the tFOV-DWI comparing to conventional fFOV-DWI (blue arrow). c: fFOV-DWI shows the focus of renal injury with low signal intensity, moderately sharp margin and recognizable lesion feature, without obvious distortions or artifacts (yellow arrow). The score for lesion conspicuity is 2.6. tFOV-DWI shows the focus of renal injury with low signal intensity, sharp margin and clear lesion feature, without obvious distortions or artifacts (yellow arrow). The score for lesion conspicuity is 3. (For interpretation of the references to colour in this figure legend, the reader is referred to the web version of this article.)

Table 4
Lesion size and corresponding diagnostic performance of fFOV-DWI and tFOV-DWI.

Rabbit Number	Lesion size (cm^2)	fFOV-DWI	tFOV-DWI
R1	0.27	Y	Y
R1	0.08	Y	Y
R2	0.30	Y	Y
R3	0.02	N	N
R4	0.13	Y	Y
R4	0.14	Y	Y
R5	0.16	Y	Y
R6	0.21	Y	Y
R7	0.08	Y	Y
R7	0.12	Y	Y
R7	0.13	N	Y
R8	0.06	N	Y
R9	0.08	N	Y
R9	0.14	Y	Y
R10	0.18	Y	Y
R11	0.09	Y	Y
R12	0.18	Y	Y
R13	0.17	Y	Y
R14	0.19	N	N

N for non-diagnostic; Y for diagnostic.

ICC values ranged from 0.775 to 0.915 for both DWI sequences (Table 8).

4. Discussion

In this study, the tFOV-DWI was investigated for early assessment of acute kidney injury and further compared with traditional fFOV-DWI. A higher percentage of renal lesions (17 out of 19) were detected in tFOV-DWI compared with fFOV-DWI (14 out of 19). Significant differences were found between ADC values in lesions and normal tissues for tFOV-DWI. Histological results were inversely correlated with ADC values of tFOV-DWI ($r = -0.97$, $P < 0.001$ for cortex; $r = -0.98$, $P < 0.001$ for medulla) and fFOV-DWI sequences ($r = -0.95$, $P < 0.001$ for cortex; $r = -0.98$, $P < 0.001$ for medulla). Significant higher subjective image scores and comparable CNR were obtained for tFOV-DWI than fFOV-DWI. ADC values were measured and there were no significant differences between measurements using fFOV-DWI and tFOV-DWI.

SS-EPI is the most commonly used strategy for abdominal DWI. However, it suffers from several problems such as distortion, image artifacts, and low-resolution. Besides, kidney images are easily affected by adjacent air-filled gastrointestinal (GI) tract [27]. Jin et al. and Riffel et al. demonstrated that targeted FOV-DWI enabled an improved image quality relative to full FOV-DWI in renal and pancreas MR Imaging in healthy volunteers [27,28]. In principle, tFOV-DWI combined with 2D excitation RF pulse lead to decreased number of k-space lines in the PE direction and significantly shorten the length of ETL depending on the ratio of desired FOV to the full FOV, thus tFOV-DWI have a targeting highlighted ability to offer considerable potential for overcoming limitations of fFOW-DWI in artifact and distortion. In this study, consistent with previous studies [29–31], artifact and distortion scores from two readers in tFOV-DWI were significantly higher than fFOV-DWI. Despite of possible reader variation for scoring image quality, excellent inter-observer agreement among all subjective image scores for two DWI sequences was obtained.

In objective image assessment, the tFOV-DWI showed a trend toward lower SNR compared with fFOV-DWI in cortex and medulla due to smaller voxel size, and this was in agreement with the literature [21]. Comparable CNRs of tFOV-DWI and fFOV-DWI were obtaining in both medulla and cortex. We believed that it was mainly due to a higher standard deviation of tFOV-DWI than fFOV-DWI, and this might also be the cause of opposite SNR results in previous studies [32,33].

Although no significant differences were observed in CNR values between tFOV-DWI and fFOV-DWI, significant higher lesion depiction scores in tFOV-DWI were obtain than in fFOV-DWI. As the human eye is the ultimate receptor for the image, subjective evaluation is considered to be the most accurate way to characterize image quality. In fact, human visual perception process is complex and consists of multi-steps including row sensory information input, signal preprocessing and a combination of sensory information and the system's inner information [34,35]. Objective measurements including CNR and SNR ignore the image content and position information and only calculate the relationship between pixels. Thus, it is difficult for those objective parameters to mimic human eyes to evaluate comprehensive characteristics

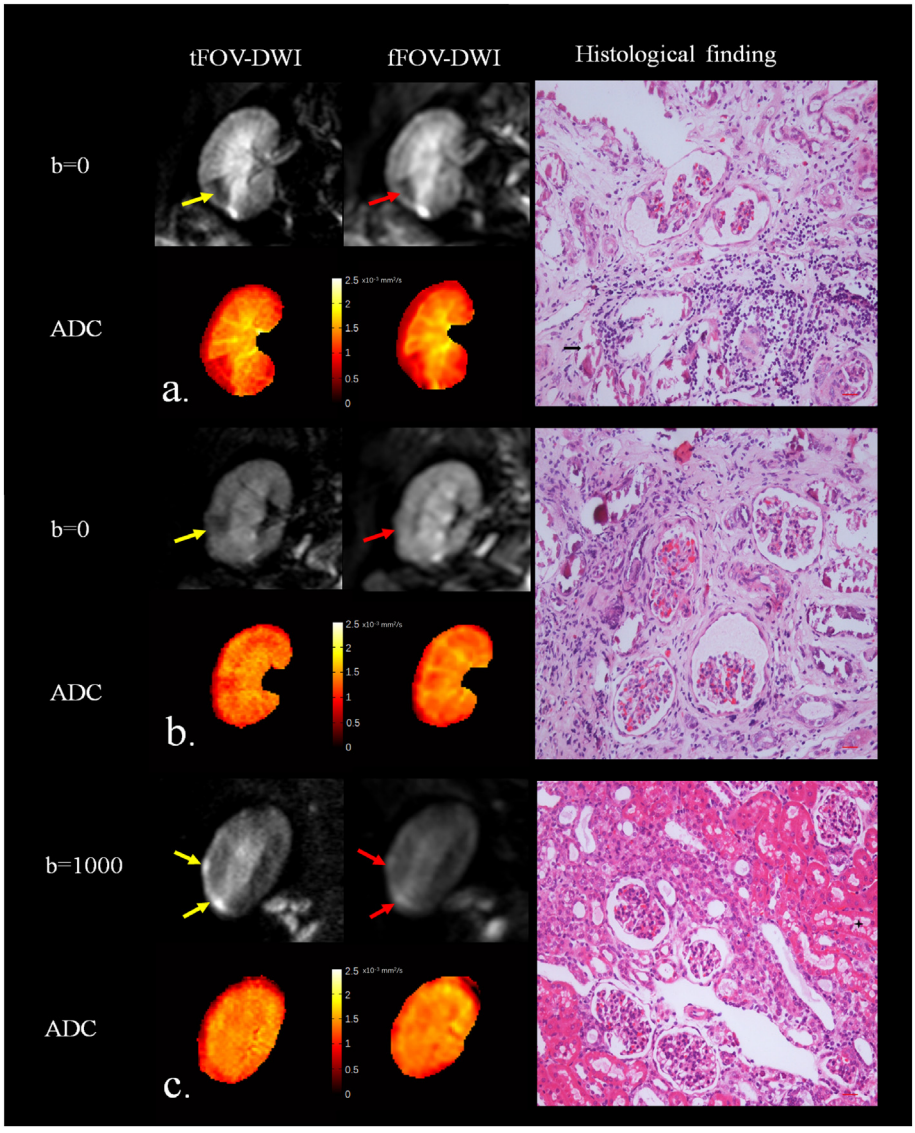

Fig. 2. Typical lesion depiction comparisons between tFOV-DWI and fFOV-DWI and corresponding ADC maps and histological findings.

Table 5
ADC comparison between normal tissue and lesion.

ADC ($\times 10^{-3}$ mm^2/s)	fFOV-DWI		tFOV-DWI	
	Cortex	Medulla	Cortex	Medulla
Normal Tissue	1.03 ± 0.06	1.59 ± 0.06	1.08 ± 0.05	1.63 ± 0.06
Lesion	0.66 ± 0.06	0.97 ± 0. 05	0.70 ± 0.03	1.02 ± 0.07
P Value[a]	< 0.001*	< 0.001*	< 0.001*	< 0.001*

n = 10 for cortex comparison; n = 7 for medulla comparison.
fFOV-DWI and tFOV-DWI indicates full FOV DWI and targeted FOV DWI, respectively.
[a] *t*-Test to compare fFOV-DWI with tFOV-DWI (*indicates significant *P*-values).

Table 6
Comparison of ADC values between fFOV-DWI and tFOV-DWI.

ADC ($\times 10^{-3}$ mm^2/s)	Normal cortex tissue	Lesion in cortex	Normal medulla tissue	Lesion in medulla
fFOV-DWI	1.03 ± 0.06	0.66 ± 0.06	1.59 ± 0.06	0.97 ± 0. 05
tFOV-DWI	1.08 ± 0.05	0.70 ± 0.03	1.63 ± 0.06	1.02 ± 0.07
P value[a]	0.12	0.08	0.14	0.07

n = 10 for cortex comparison; *n* = 7 for medulla comparison.
[a] Paired *t*-test to compare fFOV-DWI with tFOV-DWI (*indicates significant *P*-values).

of image quality.

Acquisition of high-resolution DWI in acute kidney injury is crucial because some lesions are small, shallow and difficult to demonstrate especially in their early stage. In this study, subjective lesion identification scores in tFOV-DWI were significantly higher than fFOV-DWI. Most of the lesions were detected on both DWI techniques (14/19 for fFOV-DWI; 17/19 for tFOV-DWI). However, 3 lesions missed out by fFOV-DWI with the size < 0.1 cm^2 were detected by tFOV-DWI, and this might because of the high image resolution and decreased partial volume effect in tFOV-DWI [36]. The significant improvements in image quality observed with tFOV-DWI indicated that it might enable improved early detection of AKI injuries, especially for the small injury.

DWI with quantification of ADC has been proven to be valuable in renal allografts dysfunction and renal insufficiency [37,38]. In our study, ADC values in AKI were significantly reduced compared with normal tissue for both cortex and medulla immediately after renal surgery. We believe that the ADC decrease in AKI was associated with

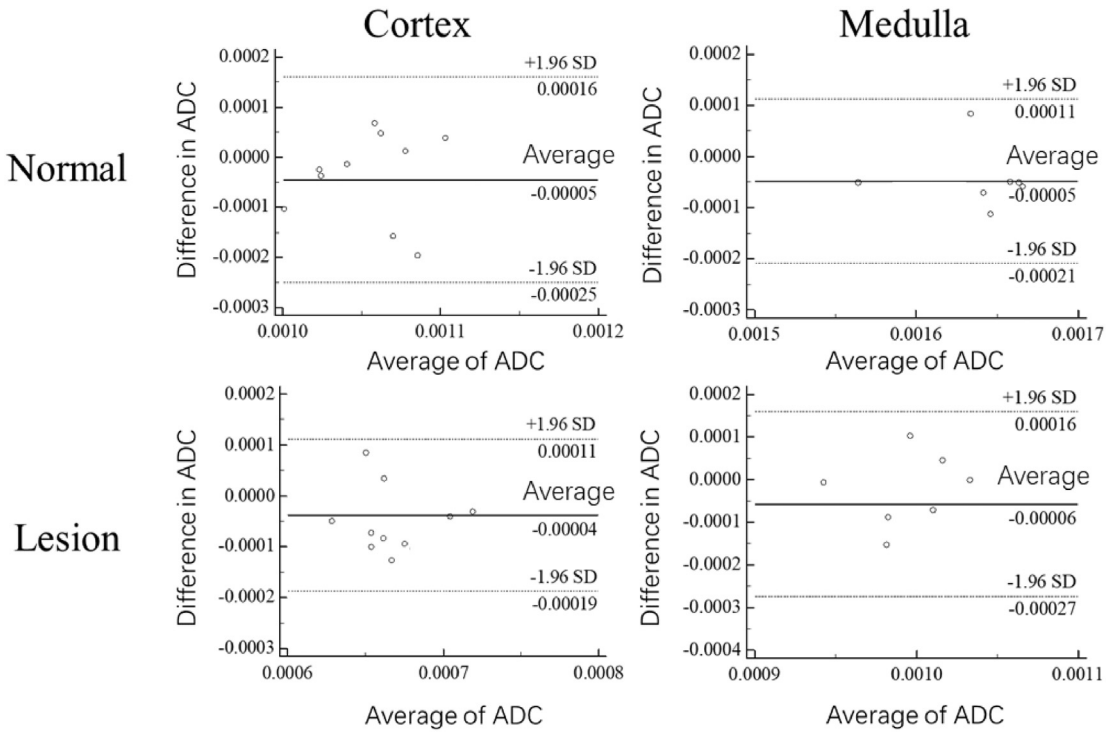

Fig. 3. Bland-Altman plots of fFOV-DWI derived ADC and tFOV-DWI derived ADC in normal cortex tissue, normal medulla tissue, medulla lesion for 14 rabbits.

Table 7
Spearman rank correlation analysis of ADC values between tFOV-DWI and fFOV-DWI and histological findings of AKI.

	fFOV-DWI	tFOV-DWI
Cortex	r = −0.95	r = −0.97
Medulla	r = −0.98	*r* = −098

$n = 20$ for cortex comparison; $n = 14$ for medulla comparison.
$P < 0.0001$ for all comparisons.

Table 8
Interobserver interclass correlation coefficient.

	DWI	ICC	CI	
Artifacts	fFOV-DWI	0.850	0.554	0.950
	tFOV-DWI	0.775	0.329	0.924
Distortion	fFOV-DWI	0.912	0.738	0.970
	tFOV-DWI	0.817	0.453	0.938
Lesion depiction	fFOV-DWI	0.829	0.492	0.943
	tFOV-DWI	0.915	0.746	0.971

n = 14 for all comparison.

inflammatory cell infiltration and cell swelling [39,40]. In clinical, ADC values may be used as noninvasive biomarkers to determine the presence of AKI in early stage.

As the reproducibility of ADC values is a major concern, ADC measurements generated from tFOV-DWI and fFOV-DWI were compared in normal cortex tissue, cortex lesion, normal medulla and medulla lesion. The mean ADC values were not significantly different between tFOV-DWI and fFOV-DWI and showed acceptable agreement. These findings were consistent with published studies in spinal cords [21] and pancreas [41].

There are some limitations in this study. We chose to examine fFOV-DWI in renal imaging and only compared with full FOV DWI sequence. Other competing approaches such as multi-shot EPI, parallel EPI and inner volume imaging were not tested. Besides, additional evaluation of the Targeted FOV DWI sequence is desirable in patients with confirmed pathologies to confirm the clinical relevance of the sequence ultimately.

5. Conclusion

In conclusion, tFOV-DWI provided visually better image quality and lesion identification than fFOV-DWI **as a noninvasive method for early assessment of acute kidney injury.**

Acknowledgements

The authors acknowledge support from the National Natural Science Foundation of China under grant [No. 81571666].

References

[1] Wijeysundera DN, Karkouti K, Dupuis JY, Rao V, Chan CT, Granton JT, et al. Derivation and validation of a simplified predictive index for renal replacement therapy after cardiac surgery. JAMA, J Am Med Assoc 2007;297(16):1801–9.
[2] Mehta RL, Kellum JA, Shah SV, Molitoris BA, Ronco C, Warnock DG, et al. Acute kidney injury network: report of an initiative to improve outcomes in acute kidney injury. Crit Care 2007;11(2).
[3] Mehta RL, Pascual MT, Soroko S, Savage BR, Himmelfarb J, Ikizler TA, et al. Spectrum of acute renal failure in the intensive care unit: the PICARD experience. Kidney Int 2004;66(4):1613–21.
[4] Leung KCW, Tonelli M, James MT. Chronic kidney disease following acute kidney injury-risk and outcomes. Nat Rev Nephrol 2013;9(2):77–85.
[5] Earley A, Miskulin D, Lamb EJ, Levey AS, Uhlig K. Estimating equations for glomerular filtration rate in the era of creatinine standardization a systematic review. Ann Intern Med 2012;156(11). (785-+).
[6] Wen XY, Murugan R, Peng ZY, Kellum JA. Pathophysiology of acute kidney injury: a new perspective. Contrib Nephrol 2010;165:39–45.
[7] Singh P, Ricksten SE, Bragadottir G, Redfors B, Nordquist L. Renal oxygenation and haemodynamics in acute kidney injury and chronic kidney disease. Clin Exp Pharmacol Physiol 2013;40(2):138–47.
[8] Notohamiprodjo M, Reiser MF, Sourbron SP. Diffusion and perfusion of the kidney. Eur J Radiol 2010;76(3):337–47.
[9] Thoeny HC, De Keyzer F, Oyen RH, Peeters RR. Diffusion-weighted MR imaging of kidneys in healthy volunteers and patients with parenchymal diseases: initial experience. Radiology 2005;235(3):911–7.
[10] Müller M, Prasad PV, Bimmler D, Kaiser A, Edelman RR. Functional imaging of the kidney by means of measurement of the apparent diffusion coefficient. Radiology 1994;193(3):711–5.
[11] Thoeny HC, Zumstein D, Simon-Zoula S, Eisenberger U, De Keyzer F, Hofmann L,

et al. Functional evaluation of transplanted kidneys with diffusion-weighted and BOLD MR imaging: initial experience. Radiology 2006;241(3):812–21.
[12] Hueper K, Rong S, Gutberlet M, Hartung D, Mengel M, Lu X, et al. T2 relaxation time and apparent diffusion coefficient for noninvasive assessment of renal pathology after acute kidney injury in mice comparison with histopathology. Invest Radiol 2013;48(12):834–42.
[13] Farzaneh F, Riederer SJ, Pelc NJ. Analysis of T2 limitations and off-resonance effects on spatial resolution and artifacts in echo-planar imaging. Magn Reson Med 1990;14(1):123–39.
[14] Morelli J, Porter D, Ai F, Gerdes C, Saettele M, Feiweier T, et al. Clinical evaluation of single-shot and readout-segmented diffusion-weighted imaging in stroke patients at 3 T. Acta Radiol 2013;54(3):299–306.
[15] Vidiri A, Minosse S, Piludu F, Curione D, Pichi B, Spriano G, et al. Feasibility study of reduced field of view diffusion-weighted magnetic resonance imaging in head and neck tumors. Acta Radiol 2016;3.
[16] Tsuchiya K, Fujikawa A, Suzuki Y. Diffusion tractography of the cervical spinal cord by using parallel imaging. Am J Neuroradiol 2005;26(2):398–400.
[17] Cercignani M, Horsfield MA, Agosta F, Filippi M. Sensitivity-encoded diffusion tensor MR imaging of the cervical cord. Am J Neuroradiol 2003;24(6):1254–6.
[18] Holdsworth SJ, Skare S, Newbould RD, Guzmann R, Blevins NH, Bammer R. Readout-segmented EPI for rapid high resolution diffusion imaging at 3T. Eur J Radiol 2008;65(1):36–46.
[19] Kim TH, Zollinger L, Shi XF, Kim SE, Rose J, Patel AA, et al. Quantification of diffusivities of the human cervical spinal cord using a 2D single-shot interleaved multisection inner volume diffusion-weighted Echo-planar imaging technique. Am J Neuroradiol 2010;31(4):682–7.
[20] Jeong EK, Kim SE, Guo JY, Kholmovski EG, Parker DL. High-resolution DTI with 2D interleaved multislice reduced FOV single-shot diffusion-weighted EPI (2D ss-rFOV-DWEPI). Magn Reson Med 2005;54(6):1575–9.
[21] Saritas EU, Cunningham CH, Lee JH, Han ET, Nishimura DG. DWI of the spinal cord with reduced FOV single-shot EPI. Magn Reson Med 2008;60(2):468–73.
[22] Dowell NG, Jenkins TM, Ciccarelli O, Miller DH, Wheeler-Kingshott CAM. Contiguous-slice zonally oblique multislice (CO-ZOOM) diffusion tensor imaging: examples of in vivo spinal cord and optic nerve applications. J Magn Reson Imaging 2009;29(2):454–60.
[23] Wilm BJ, Svensson J, Henning A, Pruessmann KP, Boesiger P, Kollias SS. Reduced field-of-view MRI using outer volume suppression for spinal cord diffusion imaging. Magn Reson Med 2007;57(3):625–30.
[24] Koyasu S, Iima M, Umeoka S, Morisawa N, Porter DA, Ito J, et al. The clinical utility of reduced-distortion readout-segmented echo-planar imaging in the head and neck region: initial experience. Eur Radiol 2014;24(12):3088–96.
[25] Tsien C, Cao Y, Chenevert T. Clinical applications for diffusion magnetic resonance imaging in radiotherapy. Semin Radiat Oncol 2014;24(3):218–26.
[26] Hallgren KA. Computing inter-rater reliability for observational data: an overview and tutorial. Tutor Quant Methods Psychol 2012;8(1):23–34.
[27] Jin N, Deng J, Zhang LJ, Zhang ZL, Lu GM, Omary RA, et al. Targeted single-shot methods for diffusion-weighted imaging in the kidneys. J Magn Reson Imaging 2011;33(6):1517–25.
[28] Riffel P, Michaely HJ, Morelli JN, Pfeuffer J, Attenberger UI, Schoenberg SO, et al. Zoomed EPI-DWI of the pancreas using two-dimensional spatially-selective radiofrequency excitation pulses. PLoS One 2014;9(3):e89468.
[29] Kim H, Lee JM, Yoon JH, Jang JY, Kim SW, Ryu JK, et al. Reduced field-of-view diffusion-weighted magnetic resonance imaging of the pancreas: comparison with conventional single-shot Echo-planar imaging. Korean J Radiol 2015;16(6):1216–25.
[30] Ma C, Li YJ, Pan CS, Wang H, Wang J, Chen SY, et al. High resolution diffusion weighted magnetic resonance imaging of the pancreas using reduced field of view single-shot echo-planar imaging at 3 T. Magn Reson Imaging 2014;32(2):125–31.
[31] Radhakrishnan R, Betts AM, Care MM, Serai S, Zhang B, Jones BV. Reduced field of view diffusion-weighted imaging in the evaluation of congenital spine malformations. J Neuroimaging 2015;26(3):273–7.
[32] Stocker D, Manoliu A, Becker AS, Barth BK, Nanz D, Klarhofer M, et al. Image quality and geometric distortion of modern diffusion-weighted imaging sequences in magnetic resonance imaging of the prostate. Invest Radiol 2018;53(4):200–6.
[33] Peng Y, Li Z, Tang H, Wang Y, Hu X, Shen Y, et al. Comparison of reduced field-of-view diffusion-weighted imaging (DWI) and conventional DWI techniques in the assessment of rectal carcinoma at 3.0 T: image quality and histological T staging. J Magn Reson Imaging 2018;47(4):967–75.
[34] Barlow HB. Vision - a computational investigation into the human representation and processing of visual information - Marr, D. J Math Psychol 1983;27(1):107–10.
[35] Haikonen PO. The cognitive approach to conscious machines. Exeter UK: Imprint Academic; 2003.
[36] Seeger A, Klose U, Bischof F, Strobel J, Ernemann U, Hauser TK. Zoomed EPI DWI of acute spinal ischemia using a parallel transmission system. Clin Neuroradiol 2016;26(2):177–82.
[37] Inoue T, Kozawa E, Okada H, Inukai K, Watanabe S, Kikuta T, et al. Noninvasive evaluation of kidney hypoxia and fibrosis using magnetic resonance imaging. J Am Soc Nephrol 2011;22(8):1429–34.
[38] Thoeny HC, De Keyzer F. Diffusion-weighted MR imaging of native and transplanted kidneys. Radiology 2011;259(1):25–38.
[39] Togao O, Doi S, Kuro-O M, Masaki T, Yorioka N, Takahashi M. Assessment of renal fibrosis with diffusion-weighted MR imaging: study with murine model of unilateral ureteral obstruction. Radiology 2010;255(3):772–80.
[40] Lebihan D, Breton E, Lallemand D, Aubin ML, Vignaud J, Lavaljeantet M. Separation of diffusion and perfusion in intravoxel incoherent motion Mr imaging. Radiology 1988;168(2):497–505.
[41] Concia M, Sprinkart AM, Penner AH, Brossart P, Gieseke J, Schild HH, et al. Diffusion-weighted magnetic resonance imaging of the pancreas: diagnostic benefit from an intravoxel incoherent motion model-based 3 b-value analysis. Invest Radiol 2014;49(2):93.